SPATIOTEMPORAL VARIATIONS AND FUTURE PROJECTIONS OF EXTREME PRECIPITATION EVENTS IN SOUTHWESTERN CHINA

LI, X. H.[1,2*] – CHEN, Z. F.[1,3] – WANG, L.[1]

[1]*School of Atmospheric Sciences, Chengdu University of Information Technology, Chengdu 610225, Sichuan, China*

[2]*Yunnan R&D Institute of Natural Disaster on Chengdu University of Information Technology, Kunming 650034, Yunnan, China*

[3]*Shiyan Meteorological Bureau, Shiyan 442000, Hubei, China*

[*]*Corresponding author*
e-mail: lixiehui325328@163.com; phone: +86-28-8563-4698

(Received 1st Jun 2023; accepted 11th Aug 2023)

Abstract. Southwestern China is a sensitive area to climate change. It is also a region where frequent extreme weather and climate events occur. In the present research, daily precipitation from 1969 to 2020 at 93 weather stations in Southwestern China, and data from nine models for the period 1995 to 2040 were used in the Coupled Model Intercomparison Project Phase 6 (CMIP6) to calculate 11 Extreme Precipitation Indices (EPIs) in four sub-regions. Moreover, the annual change rate, spatiotemporal variation trend, and mean change of extreme precipitation events in the four sub-regions were determined in the intermediate emission of Shared Socio-economic Pathway (SSP2-4.5) scenario for a historical period and from 2021 to 2040. The results showed that between 1969-2020, Southwestern China presented a decrease in the number of continuous precipitation days, increasing precipitation intensity, and extreme precipitation events. The overall analysis of the annual change rates of 11 EPIs under the SSP2-4.5 scenario in the next 20 years showed that the number of consecutive dry and wet days will decrease, and the amount of precipitation on wet days, as well as the frequency and intensity of extreme precipitation will increase. However, obvious differences between historical and projected values in four sub-regions were observed.
Keywords: *EPIs, trend changes, CMIP6, Taylor diagram, skill score, SSP2-4.5 scenario, model ensemble mean, different sub-regions*

Introduction

The Intergovernmental Panel on Climate Change (IPCC) Working Group I contribution to the Sixth Assessment Report (AR6) states that in the 21st century, warming caused by greenhouse gases will cause precipitation changes with significant regional and seasonal differences (high confidence). In addition, precipitation may increase in most monsoon regions (IPCC, 2021; Zhou, 2021). Studies performed by Allen and Ingram (2012) and Wentz et al. (2007) showed that for every 1 K increase in global temperature, the water vapor content of the atmosphere will increase by 7%. The increase in atmospheric humidity will augment the intensity of extreme precipitations. Currently, extreme climate events such as rainstorms and floods are of great concern (Sun, 2018). The change of extreme climate events has always been the focus of the IPCC Assessment. For the first time, the IPCC AR6 report includes a chapter (Chapter 11) with a systematic evaluation of extreme precipitation events including heavy precipitation and floods. This assessment suggested that the frequency and intensity of global-scale land-based intense precipitation events may have increased since the mid-20th century. On a continental scale,

http://www.aloki.hu ● ISSN 1589 1623 (Print) ● ISSN 1785 0037 (Online)
DOI: http://dx.doi.org/10.15666/aeer/2106_53895414

in addition to Europe and North America, intense precipitation events may have increased and intensified in the Asian region, and they are likely to become stronger and more frequent as global warming intensifies. So far, CMIP6 models have been used to project the future trend, days with different levels of precipitation, duration, intensity, and frequency of extreme precipitation events in different parts of the world. Scholars have assessed the projection uncertainty and compared the simulation performance of different models. Various projections of extreme precipitation events for future periods on different time scales and in different regions have been obtained (Srivastava et al., 2020; Chen et al., 2020; Gupta et al., 2020; Agel and Barlow, 2020; Li et al., 2020; Scoccimarro and Gualdi, 2020; Klutse et al., 2021; Zarrin and Dadashi-Roudbari, 2021; Akinsanola et al., 2021; Dong and Dong, 2021).

China is susceptible to the influence of global climate change, and temperature usually increases at rates significantly higher than the worldwide average. From 1961 to 2020, China's annual average precipitation showed an increasing trend, with an average interannual increasing rate of 5.1 mm/10 a. Specifically, China's annual average precipitation increased between the 1980s and 1990s, and it was generally lower in the first decade of the 21st century. Since 2012, China has witnessed a continuous increase in precipitation. However, there has been a significant regional variation in precipitation within China. The annual precipitation increased significantly in the central and northern parts of Northeastern China, in most parts of the Yangtze-Huaihe to Jiangnan region, central and northern parts of the Qinghai-Tibet Plateau, and central and western parts of Northwestern China. By contrast, the annual precipitation decreased in the southern part of Northwestern China, the southeastern part of North China, most parts of the Yellow River and Huai River, eastern and southern parts of Southwestern China, and the southeastern part of Northwestern China. In the past 60 years (1961-2020), China has experienced an increase in extreme heavy precipitation events in both intensity and frequency, which directly enhance climate risk (China Meteorological Administration Climate Change Centre, 2021).

Considering the additional warming of China's climate in the future, Yang et al. (2021) performed projections using the CMIP6 multi-model ensemble under the SSP2-4.5 and SSP5-8.5 (high radiation forcing and traditional fossil fuel-driven development path) scenarios. Their results indicated a 17% and 30% increase, respectively, in annual precipitation by the end of this century as compared to the reference period 1995-2014. These numbers surpass the global annual precipitation average. Affected by climate warming, China's future extreme precipitation events will also show an overall increasing trend. However, regional variations are expected. For example, Ai et al. (2021) used the CMIP6 multi-model median ensemble to project spring extreme precipitation indices in China and its eight sub-regions from 2021 to 2100. Their data indicated that only a few models showed a good performance. The spatial patterns in the total annual wet-day precipitation (PRCPTOT), very wet days (R95p), and the number of heavy precipitation days (R10) reflected similar changes along a north-to-south gradient, whereas the changes in the consecutive dry days (CDD) reflected the opposite pattern. In most regions, these spatial differences were dependent on the index type, and the projected changes in percentile indices were stronger than the projected changes in absolute indices. Xu et al. (2022) studied the future changes in precipitation extremes across China based on CMIP6 models. The results showed that the multi-model median ensembles of 14 CMIP6 models generally exhibited superior performance in simulating the EPIs as compared to CMIP5. By the end of the 21st century, PRCPTOT is expected to increase over most regions of

http://www.aloki.hu ● ISSN 1589 1623 (Print) ● ISSN 1785 0037 (Online)
DOI: http://dx.doi.org/10.15666/aeer/2106_53895414

China and the largest increases will be located over the northwestern China (NWC, 36°-46°N, 75°-111°E) and northern China (NC, 36°-46°N, 111°-119°E) regions, especially under the SSP5-8.5 scenario. The changes in R95p and the max 5-day precipitation amount (RX5day) were similar to those in PRCPTOT, with the largest increases centered over NWC and NC. However, a relatively high model fitting indicated that CDD was expected to significantly decrease in the dry NWC and NC regions by the end of this century. Although the number of very heavy precipitation days (R20) was projected to generally increase over most regions of China as PRCPTOT, some parts of the NWC will experience decreases in R20. The largest increase will be observed in the eastern China (EC, 27°-36°N, 116°-122°E) and southern China (SC, 20°-27°N, 106°-120°E). It was also observed that the model showed a better level of agreement under the SSP5-8.5 scenario as compared to the SSP2-4.5 scenario.

Southwestern China is located in the southeastern part of the Tibetan Plateau, displays a complex topography and structure, it is one of the seven natural geographical divisions in China. As a result of the combined influence of the South Asian monsoon, the East Asian monsoon, and the plateau monsoon, its climate is unique. This is an area sensitive and vulnerable to climate change, and also one of the regions where extreme weather and climate events occur most frequently (Wu et al., 2012). Some scholars have discussed historical extreme precipitation events in Southwestern China. For example, Yuan et al. (2014) found a generally increasing trend in extreme precipitation events in Southwestern China from 1962 to 2012; however, the increase was insignificant. Besides, considerable heterogeneity in the distribution of extreme precipitation events was observed within this region. Ding (2014) studied the spatial and temporal variations of extreme precipitation events in Southwestern China from 1960 to 2011. The results showed an increase in the frequency of extreme precipitation since the 1960s. However, a significant interdecadal difference was observed in the frequency of extreme precipitation events across the regions. Luo et al. (2015) showed that although the total precipitation and the longest number of continuous days without rain decreased in Southwestern China between 1970 and 2010, the frequency of strong precipitation and intensity increased. In addition, a significant regional difference was noted in the spatial variation of extreme precipitation. Lu et al. (2017) used the daily precipitation series at 98 meteorological stations from 1961 to 2015. The integrated precipitation indicator system was analyzed. As for the spatial distribution morphology, precipitation events were more frequent in the south and east and less frequent in the north and west in Southwestern China. Xue et al. (2022) used daily precipitation data from 116 meteorological stations in Southwestern China from 1976 to 2017 to analyze the spatial and temporal distribution features of different grades of precipitation in the summer. They further showed the dominance of moderate rain in the summer among all grades of average precipitation. Because of topographic factors and atmospheric circulation, light and moderate rains were more frequent in the middle as compared to the other two sides, while heavy rain and rainstorms were more frequent in the east than in the west. A progressive increase in the interannual variation of precipitation of rainstorms in Tibet and western Sichuan was observed. In eastern Sichuan and Chongqing, the interannual variation presented a significant increase. Also, in eastern Yunnan and most parts of Guizhou, a progressive decrease in interannual variation occurred.

Recently, some scholars reported the use of the CMIP5 model to project precipitation in the wet and dry seasons (Zhang et al., 2015) and the annual and seasonable average precipitation in the 21st century in Southwestern China (Zhang et al., 2016; Hu et al.,

http://www.aloki.hu ● ISSN 1589 1623 (Print) ● ISSN 1785 0037 (Online)
DOI: http://dx.doi.org/10.15666/aeer/2106_53895414

2020a). However, few refined projections have been carried out for several EPIs and zoning concerning extreme precipitation events in Southwestern China. For example, Hu et al. (2020b) employed the RegCM4.0 and the BCC_CSM1.1 data for future change projections of consecutive climate events in Southwestern China. Under the Representative Concentration Pathway (RCP4.5) scenario, both the greatest consecutive wet days (GCWD) and greatest consecutive dry days (GCDD) showed a weak increasing trend from 2025 to 2055. The CMIP6 incorporates the largest number of climate models, has the most reasonable experimental design, and provides the largest volume of simulation data ever since the CMIP was first launched over 20 years ago. Wang et al. (2021) evaluated the simulation performance of CMIP6 models for China's extreme precipitation. The results showed that compared with CMIP5 models, CMIP6 had better improvement and enhancement of climate change projections including climate mean state, climate variability, and time skill (TS) scores of homologous models. However, differences were observed in the improvement degree across the regions and in different EPIs.

Because of the influence of the working mechanism, configuration of initial conditions, and resolution, the precision of simulations for a given set of regions may vary in different CMIP models (Zhou et al., 2020). Zhang et al. (2015) applied different CMIP5 models for precipitation simulation and projection in dry and wet seasons in Southwestern China. They found that ACCESS1-0, ACCESS1-3, CanESM2, MIROC5, and IPSL-CM5A-LR models displayed an outstanding performance. In contrast, the multimodel ensemble showed a tendency to overestimate precipitation in dry and wet seasons in most parts of Southwestern China. Zhang et al. (2016) carried out a comparative analysis of changes in average precipitation in Southwestern China in the 21st century through CMIP5 multimodel ensemble projection. They found that the MIROC5 model had a better simulation performance for average precipitation in summer. Cheng (2019) employed CMIP5 models to project spatial and temporal characteristics of precipitation in the upper reaches of the Yangtze River in Southwestern China from 1961 to 2005. MPI-ESM-LR was identified as one of the eight optimal CMIP5 models. Furthermore, it was revealed that measured precipitation was lower than simulated values obtained with any single model. However, a consistent precipitation trend was noted between simulated and measured values. Xiang et al. (2021) assessed the performance of CMIP6 models to simulate extreme precipitation in the major regions of China. It was found that 20 GCMs produced significantly different simulations of five EPIs (annual maximum 5-day consecutive precipitation (RX5day), the annual sum of daily precipitation>95th percentile (R95P), the annual sum of daily precipitation>99th percentile (R99P), extreme precipitation contribution rate (P95T), and simple daily precipitation intensity (SDII)). In addition, the simulation results also varied across regions. The INM-CM4-8 model presented the highest temporal correlation coefficient. However, GCMs generally displayed poor simulation performance for the five EPIs in Southwestern China. Wang et al. (2021) assessed the simulation performance of the CMIP6 models for the mean climate state of China's eight EPIs. The top-ranking models in terms of TS score were CanESM5, ACCESS-CM2, CESM2, INM-CM5-0, and NESM3.

Compared with a continuous temperature rise in the long term, changes in extreme precipitation events are more likely to cause casualties and property damage. For this reason, accurate simulation and projection of extreme precipitation are of particular importance. Each region's extreme precipitation events have their respective distribution pattern and evolutionary trend. It is important to conduct a refined projection of extreme

http://www.aloki.hu ● ISSN 1589 1623 (Print) ● ISSN 1785 0037 (Online)
DOI: http://dx.doi.org/10.15666/aeer/2106_53895414

precipitation events in the context of global warming in Southwestern China, which lies close to the eastern Tibetan Plateau, has a complex topography, and distinctive weather and climate features. In the present research, we selected nine models in CMIP6 to obtain 11 EPIs for Southwestern China. We analyzed spatiotemporal variations of historical extreme precipitation events during 1969-2020 in four sub-regions divided according to their meteorological and topographical characteristics. Also, we projected the change trends of extreme precipitation events for the period 2021-2040 under the SSP2-4.5 scenario. Moreover, we performed a comparative analysis of past and future extreme precipitation events in four sub-regions. Our results can provide an important scientific reference for a more comprehensive understanding of extreme precipitation events in the near future (2021-2040) in Southwestern China. These data can be used by relevant departments to formulate disaster prevention and mitigation measures in the context of global warming.

Data and methods

Study area

Southwestern China (21°08’～34°19’ N, 97°21’～110°11’ E) borders South Central China to the east, Vietnam, Laos, and Burma to the south, Tibet Plateau to the west, and Northwestern China to the north. It displays a downward-sloped terrain from the northwest to the southeast. Southwestern China extends over the first and second steps of China’s ladder topography, resulting in a diversity of climate features. In this region, cold and warm air masses converge. The summer is hot and humid; the winter is cold and rainy; and the spring and autumn are cloudy and foggy with little sunshine. In this region, the annual precipitation shows uneven spatial distribution with significant regional differences. In general, heavy and light precipitation events occur in the southeast and the northwest, respectively. Also, as a result of the topography and orientation of the mountain range, rainy and rainless regions arrange in alternating order. Southwestern China is known to be particularly vulnerable to weather and climate change. Frequent rainstorms and floods plus weak disaster resilience have caused significant economic losses in this area (Yan et al., 2021). In the present research, Southwestern China was divided into four landform units based on climate and hydrologic conditions, geographical location from north to south, as well as altitude. These units include (a) Zoigê Plateau (ZP), which covers part of northern Sichuan; (b) Hengduan Mountains (HMs) in western and southern Sichuan and northern Yunnan; (c) Sichuan Basin (SB), enclosing most of Chongqing City and eastern and central Sichuan; and (d) Yunnan-Guizhou Plateau (YGP), covering most of Guizhou as well as part of southern Yunnan.

Data

Daily precipitation data for the period 1969 to 2020 were obtained from the China Meteorological Data Service Center (MDSCC) (http://data.cma.cn). 93 weather stations located in Southwestern China were chosen for the study. To ensure the accuracy, homogeneity, and continuity of weather data, data quality control, linear regression, and interpolation methods were used (Li et al., 2020). The digital elevation model (DEM) information was obtained from the SRTM data (http://www.cgiar-csi.org/) published by the National Imagery and Mapping Agency. *Figure 1* displays the geographical locations of the 93 weather stations and DEM of the four geographical divisions in Southwestern

http://www.aloki.hu ● ISSN 1589 1623 (Print) ● ISSN 1785 0037 (Online)
DOI: http://dx.doi.org/10.15666/aeer/2106_53895414

China. *Table 1* shows the distributions of the 93 weather stations in the four geographical divisions. According to *Table 1*, four stations are located in the ZP, 22 in the HMs, 23 in SB, and 44 in the YGP (Chen et al., 2022).

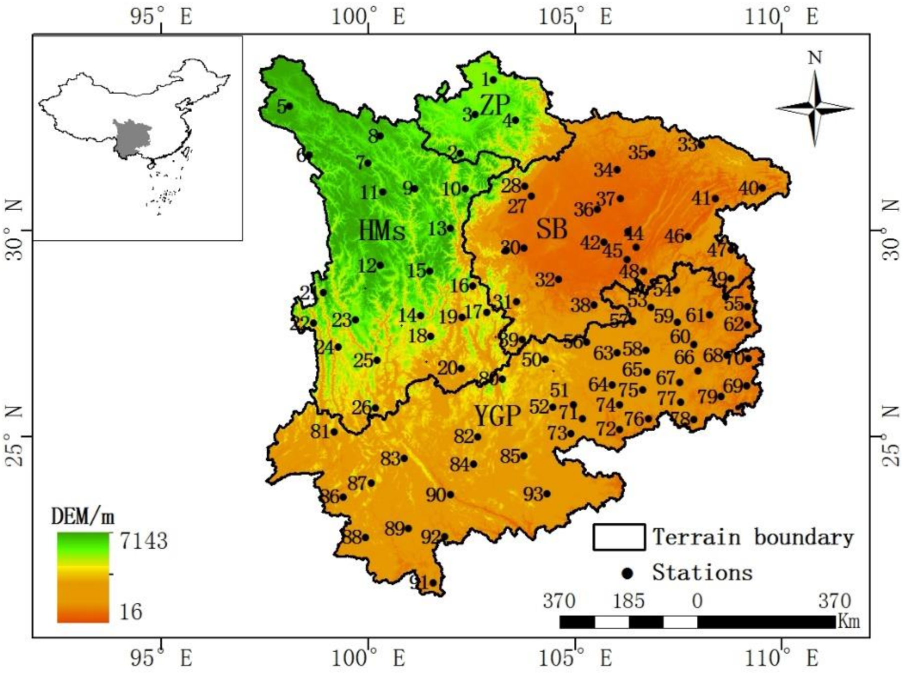

Figure 1. *Topographical division and spatial distribution of weather stations in Southwestern China*

Table 1. *Distribution in four terrain zones of 93 weather stations studied in the present research*

Topographical Division	Numbers and names of weather stations
ZP (Zoige Plateau)	1 Zoige, 2 MaErKang, 3 HongYuan, 4 SongPan
HMs (Hengduan Mountains)	5 ShiQu, 6 DeGe, 7 GanZi, 8 SeDa, 9 DaoFu, 10 XiaoJin, 11 XinLong, 12 DaoCheng, 13 KangDing, 14 MuLi, 15 JiuLong, 16 YueXi, 17 ZhaoJue, 18 YanYuan, 19 XiChang, 20 HuiLi, 21 DeQin, 22 GongShan, 23 Shangri-La, 24 WeiXi, 25 LiJiang, 26 DaLi
SB (Sichuan Basin)	27 WenJiang, 28 DuJiangYan, 29 EMeiShan, 30 LeShan, 31 LeiBo, 32 YiBin, 33 WanYuan, 34 LangZhong, 35 BaZhong, 36 SuiNing, 37 GaoPing, 38 XuYong, 39 ZhaoTong, 40 FengJie, 41 WanZhou, 42 DaZu, 43 HeChuan, 44 ShaPingBa, 45 JiangJing, 46 FengDu, 47 QianJiang, 48 QiJiang, 49 YouYang
YGP (Yunnan-Guizhou Plateau)	50 WeiNing, 51 PuAn, 52 PanXian, 53 TongZi, 54 ZhengAn, 55 SongTao, 56 BiJie, 57 HuaiRen, 58 XiFeng, 59 MeiTan, 60 YuQing, 61 SiNan, 62 TongRen, 63 QianXi, 64 AnShun, 65 GuiYang, 66 KaiLi, 67 DuYun, 68 SanSui, 69 LiPing, 70 TianZhu, 71 XingRen, 72 WangMo, 73 XingYi, 74 ZiYun, 75 HuiShui, 76 LuoDian, 77 DuShan, 78 LiBo, 79 RongJiang, 80 HuiZe, 81 BaoShan, 82 KunMing, 83 JingDong, 84 YuXi, 85 LuXi, 86 GengMa, 87 LinCang, 88 LanCang, 89 SiMang, 90 YuanJiang, 91 MengLa, 92 JiangCheng, 93 YanShan

http://www.aloki.hu ● ISSN 1589 1623 (Print) ● ISSN 1785 0037 (Online)
DOI: http://dx.doi.org/10.15666/aeer/2106_53895414

Considering previous reports and data completeness, we selected 9 CMIP6 models with relatively good simulation performance to conduct precipitation projections in Southwestern China. *Table 2* shows the basic information of the 9 selected models. These data were obtained from the website https://esgf-node.llnl.gov/search/cmip6/. Considering differences in spatial resolution of each model and to facilitate model comparison, we interpolated daily precipitation with a spatial resolution of 0.5° × 0.5° using the bilinear interpolation method. At the same time, data from each model were uniformly interpolated to the 93 weather stations. Later, 11 EPIs were calculated, and Taylor diagrams and skill score results were used to assess the degree of fitting between the modeled and observed data in the historical base period. Finally, the models with good simulation performance were selected to project and compare the spatiotemporal change trends of 11 EPIs in Southwestern China. The time-series data covered the period 1995-2040. The interval 1995-2014 represented the historical base period, and corresponding data were used to assess the model's simulation performance. Data for the period 2020-2040 were used for near-future projections considering: (1) SSP2-4.5 is an updated version of the RCP4.5 scenario in CMIP5 and combines intermediate social vulnerability with intermediate radioactive forcing. Also, it is usually used as a CMIP6 reference scenario and is the most important and intensively discussed scenario in relevant research (Jiang et al., 2020). (2) Since the reform and opening-up, China has experienced rapid economic growth and development. This situation has resulted in severe damage to the urban eco-environment. The SSP2-4.5 scenario properly represents China's national conditions. (3) The IPCC AR6 report indicated considerable uncertainty in the near-term precipitation projection because of the influence of the internal variability of the climate system, model uncertainty, natural and anthropogenic aerosol emissions (medium confidence), and no significant differences in precipitation variability across SSPs scenarios in the near-term projection (high confidence) (IPCC, 2021). Therefore, in the present investigation, we selected SSP2-4.5 as the future scenario.

Table 2. *Basic information of 9 models in CMIP6 chosen for future projections*

Number	Model name	Institution and country	Spatial resolution (grid points, Lon×Lat)
1	ACCESS-CM2	Commonwealth Scientific and Industrial Research Organization, Australia	192×144
2	CanESM5	Canadian Center for Climate Modelling and Analysis, Canada	128×64
3	CESM2	National Center for Atmospheric Research, USA	288×192
4	INM-CM4-8	Institute for Numerical Mathematics, Russia	180×120
5	INM-CM5-0	Institute for Numerical Mathematics, Russia	180×120
6	IPSL-CM6A-LR	Institute Pierre Simon Laplace, France	144×143
7	MIROC6	Japan Agency for Marine-Earth Science and Technology, Japan	256×128
8	MPI-ESM1-2-LR	Max Planck Institute for Meteorology, Germany	192×96
9	NESM3	Nanjing University of Information Science and Technology, China	192×96

http://www.aloki.hu ● ISSN 1589 1623 (Print) ● ISSN 1785 0037 (Online)
DOI: http://dx.doi.org/10.15666/aeer/2106_53895414

Methods

Extreme precipitation index

Extreme climate indices should be chosen over average values when monitoring, detecting, and analyzing the impact of climate change (Peterson et al., 2008). Herein, 11 EPIs were selected to analyze the characteristics of past and future extreme precipitation events in Southwestern China (*Table 3*). The EPIs were recommended by the World Meteorological Organization (WMO) and calculated by using the RClimDex (1.0) software developed by Xuebin Zhang and Feng Yang (http://etccdi.pacificclimate.org) (Zhang and Yang, 2004; Liu and Xu, 2014).

Table 3. *List of the 11 selected EPIs*

No.	Indices	Descriptive names/Units	Definitions
1	CDD	Consecutive dry days/d	Maximum number of consecutive days with DP (daily precipitation) <1 mm
2	CWD	Consecutive wet days/d	Maximum number of consecutive days with DP ≥1 mm
3	PRCPTOT	Annual total wet-day precipitation/mm	Annual total precipitation on wet days (DP ≥1 mm)
4	R10	Number of heavy precipitation days/d	Annual count of days when DP ≥10 mm
5	R20	Number of very heavy precipitation days/d	Annual count of days when DP ≥20 mm
6	R50	Number of rainstorm days/d	Annual count of days when DP ≥50 mm
7	R95p	Very wet days/mm	Annual total precipitation when DP >95th percentile
8	R99p	Extremely wet days/mm	Annual total precipitation when DP >99th percentile
9	RX1	Max 1-day precipitation amount/mm	Monthly maximum 1-day precipitation
10	RX5	Max 5-day precipitation amount/mm	Monthly maximum consecutive 5-day precipitation
11	SDII	Simple daily intensity index/(mm/d)	Annual total precipitation divided by the number of wet days (DP ≥1 mm)

Taylor diagram and skill score

The Taylor diagram presents three statistics: (a) the spatial correlation coefficient (R) between the simulated and the observed value; (b) the standard deviation ratio ($STDR$), which is the ratio of the standard deviation of the test field to that of the observed field; and (c) root mean square error ($RMSE$) of the simulated value relative to the observed field (Taylor, 2001; Zhang et al., 2015; Jiang and Chen, 2021). The differences between the simulated results and the reference data can be observed intuitively. Taylor diagram offers a comprehensive reflection of the simulation performance of the model. Thus, we first plotted the Taylor diagram for 9 selected single models and nine-model ensemble mean (MEM-9) to assess their simulation performance for 11 EPIs in Southwestern China. Moreover, to quantitatively describe the simulation performance of the models, the skill score (S) was also selected according to Taylor (2001) to quantitatively evaluate the simulation ability of nine single models and MEM-9 to 11 EPIs. *Equation (1)* displays the formula used for this purpose (Zhang et al., 2015):

http://www.aloki.hu ● ISSN 1589 1623 (Print) ● ISSN 1785 0037 (Online)
DOI: http://dx.doi.org/10.15666/aeer/2106_53895414

$$S = \frac{4(1+R)^4}{(STDR + \frac{1}{STDR})^2 (1+R_0)^4} \qquad \text{(Eq.1)}$$

Where R is the correlation coefficient between the simulated and the observed value; R_0 represents the maximum potential correlation coefficient that can be obtained; and *STDR* indicates the standard deviation ratio. When the variance of the simulated value is close to the variance of the observed value, the closer the spatial correlation coefficient between the simulated and the observed value is to R_0, the closer S is to 1; when the variance ratio is close to 0 or infinity, the correlation coefficient is close to -1, and S is close to 0. The larger the S, the better the simulation ability of the models. According to the Taylor diagram and skill score results, models with better simulation performance were selected to project the spatiotemporal change trends of future extreme precipitation events.

Results

Spatiotemporal variation of extreme precipitation events from 1969 to 2020

Interdecadal variation

As seen in the interannual change trends of EPIs in Southwestern China from 1969 to 2020 (*Figure 2*), the interdecadal change trend rates of the 11 EPIs were 0.26 d/10 a (CDD), -0.18 d/10 a (CWD), -5.78 mm/10 a (PRCPTOT), -0.28 d/10 a (R10), -0.09 d/10 a (R20), 0.02 d/10 a (R50), 8.88 mm/10 a (R95p), 4.58 mm/10 a (R99p), 0.47 mm/10 a (RX1), 0.35 mm/10 a (RX5) and 0.09 (mm/d)/10 a (SDII), where CWD and R99p were significant at the 0.01 level, and R95p and SDII at the 0.05 level. CWD showed a decreasing trend, while R95p, R99p and SDII showed an increasing trend, indicating a continuous decrease in precipitation days, but increasing precipitation intensity and increasing extreme precipitation events in the past 52 years in Southwestern China.

In terms of interdecadal anomaly change relative to 1969-2020 (*Table 4*), the CDD of 11 EPIs showed an increasing trend in the 1970s and from the 2010s to 2020s, and a decreasing trend in the 1980s to 1990s; CWD showed an increasing trend in the 1970s to 1990s and a decreasing trend in the 2010s to 2020s; PRCPTOT, R10, and R20 all showed an increasing trend in the 1970s and 1990s, but a decreasing trend in the 1980s and from the 2010s to 2020s; R50, R95p, and R99p all showed a decreasing trend in the 1970s to 1980s and the 2010s, while they showed an increasing trend in the 1990s and the 2020s; RX1 showed a decreasing trend in the 1970s to 1980s and an increasing trend in the 1990s to 2020s; RX5 showed an increasing trend in the 1980s to 1990s, and a decreasing trend in the 1970s and from the 2010s to 2020s; SDII showed a decreasing trend in the 1970s to 1980s, and an increasing trend in the 1990s to 2020s. Among them, the increasing trend of PRCPTOT was very obvious in the 1970s and 1990s, with 15.02 and 21.73 respectively, while the decreasing trend was most obvious in the 2010s, with -22.11; The decreasing trends of R95p and R99p in the 1970s were very significant, at -16.65 and -12.96, respectively, while the increasing trends in the 1920s were very significant, at 26.78 and 11.57, respectively.

The four sub-regions also showed different degrees of extreme precipitation. *Table 5* displays the mean values for each index. Data indicated that the highest CDD value corresponded to ZP.

http://www.aloki.hu ● ISSN 1589 1623 (Print) ● ISSN 1785 0037 (Online)
DOI: http://dx.doi.org/10.15666/aeer/2106_53895414

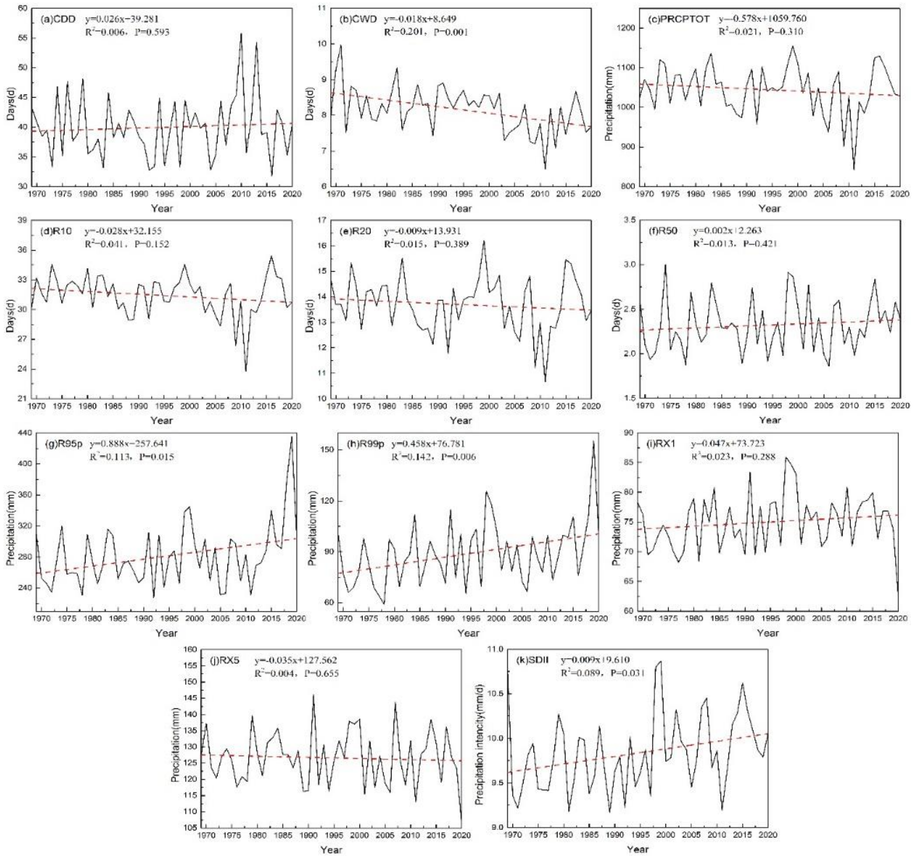

Figure 2. *Temporal variation trends of 11 EPIs in Southwestern China from 1969 to 2020. (a) CDD (b) CWD (c) PRCPTOT (d) R10 (e) R20 (f) R50 (g) R95p (h) R99p (i) RX1 (j) RX5 (k) SDII*

Table 4. *Interdecadal anomaly of 11 EPIs relative to 1969-2020*

Anomaly	CDD	CWD	PRCPTOT	R10	R20	R50	R95p	R99p	RX1	RX5	SDII
1970s	0.68	0.32	15.02	0.88	0.25	-0.09	-16.65	-12.96	-2.88	-0.55	-0.22
1980s	-1.00	0.13	-1.80	-0.05	-0.22	-0.01	-9.38	-2.44	-0.12	0.66	-0.17
1990s	-1.83	0.35	21.73	0.63	0.27	0.05	2.71	5.08	1.86	2.11	0.03
2010s	0.14	-0.33	-22.11	-0.90	-0.22	-0.04	-9.05	-3.58	0.49	-1.33	0.10
2020s	1.53	-0.40	-9.69	-0.39	-0.17	0.05	26.78	11.57	0.29	-0.87	0.15

Table 5. *Mean value of 11 EPIs in different sub-regions from 1969 to 2020*

Sub-region average	CDD(d)	CWD(d)	PRCPTOT(mm)	R10(d)	R20(d)	R50(d)
ZP (Zoige Plateau)	47.399	8.484	714.596	22.314	4.924	0.060
HMs (Hengduan Mountains)	9.650	9.650	828.864	27.073	8.951	0.715
SB (Sichuan Basin)	28.335	6.725	1080.027	29.863	14.257	3.174
YGP (Yunnan-Guizhou Plateau)	33.541	8.136	1163.592	35.248	16.577	2.886
Sub-region average	**R95p(mm)**	**R99p(mm)**	**RX1(mm)**	**RX5(mm)**	**SDII(mm/d)**	
ZP (Zoige Plateau)	141.791	39.720	33.264	67.198	6.460	
HMs (Hengduan Mountains)	177.545	50.157	44.575	91.434	8.178	
SB (Sichuan Basin)	333.991	111.327	94.197	147.417	10.474	
YGP (Yunnan-Guizhou Plateau)	318.038	101.058	82.634	136.599	10.638	

http://www.aloki.hu ● ISSN 1589 1623 (Print) ● ISSN 1785 0037 (Online)
DOI: http://dx.doi.org/10.15666/aeer/2106_53895414

In addition, PRCPTOT and the frequency of extreme precipitation events were lower in ZP than in other sub-regions, as well as precipitation intensity. Moreover, the smallest CDD and highest CWD corresponded to HMs. PRCPTOT and the intensity and frequency of extreme precipitation events were higher in HMs than in ZP but lower than those of other sub-regions. A lower CDD and the lowest CWD were observed in SB. PRCPTOT and the frequency of extreme precipitation events were also higher in SB as compared to HMs and ZP. Also, the highest intensity of extreme precipitation was found in SB. YGP displayed a larger CDD than that in HMs and SB, as well as shorter CWD as compared to the corresponding values in HMs and ZP. PRCPTOT and the frequency of extreme precipitation events presented the highest values in YGP. The intensity of extreme precipitation events was also higher in YGP. Among the four geographical divisions (*Figure 1*), the highest and lowest elevations corresponded to northwestern Southwestern China (ZP and HMs) and eastern Southwestern China (SB and northeast YGB), respectively. The population density and urbanization rate in the east were significantly higher than those in the west. As seen above, extreme precipitation events are substantially influenced by human activities. The precipitation is usually more intense in regions that are densely populated and with higher urbanization rates (SB and YGP). Besides, extreme precipitation events occur at a higher frequency and a higher intensity in those regions.

Spatial variations

The spatial distribution of the regression coefficient (*RC*) in 93 weather stations in Southwestern China for 52 years is shown in *Figure 3*. The significance of spatial change rate of 11 EPIs was tested in all the stations. Table 6 shows the spatial average change rate (SACR) of 11 EPIs in Southwestern China and four different sub-regions.

As seen in *Figure 3* and *Table 6*, the SACR of CDD in Southwestern China was 0.26 d/10 a. With respect to different sub-regions, HMs presented the largest SACR, with a value of 0.73 d/10 a. The smallest SACR was found in ZP (-1.32 d/10a), which showed a decreasing trend. The SACR of CWD decreased in all sub-regions and presented a value of -0.18 d/10 a. In addition, the highest decrease in PRCPTOT corresponded to YGP (-16.02 mm/10 a), while ZP showed an increasing trend in PRCPTOT (12.60 mm/10 a). It was also observed that PRCPTOT decreased from northwest to southeast. R10 and R20 decreased most significantly in YGP and increased in ZP and HMs. Also, both indices decreased from northwest to southeast. The SACR of R50 showed a consistently increasing trend in Southwestern China. A similar trend was also observed in R95p and R99p, with the largest variation in SB (9.68 mm/10 a, 5.26 mm/10 a). The SACR of RX1 was -2.1 mm/10 a, and it decreased most dramatically in SB, reaching -0.9 mm/10 a. On the contrary, SACR of RX1 increased in ZP (1.53 mm/10 a) and HMs (0.32 mm/10 a). The SACR of RX5 was negative in the four sub-regions. The SACR of SDII showed an increasing trend in all parts of Southwestern China; however, the highest growth was observed in ZP and HMs, where values of 0.10 (mm/d)/10 a were determined. Taking into account the distribution of SACR at these stations during 52 years, it can be said that CDD increased and CWD decreased at different stations in Southwestern China. PRCPTOT decreased from northwest to southeast. However, extreme precipitation events occurred more frequently over time. The frequency of extreme precipitation events increased most dramatically in HMs. Among the 93 meteorological stations, the proportion of stations where the SACR of 11 EPIs were significant at the 0.05 level were

http://www.aloki.hu ● ISSN 1589 1623 (Print) ● ISSN 1785 0037 (Online)
DOI: http://dx.doi.org/10.15666/aeer/2106_53895414

low (all below 50% for the 11 EPIs). Therefore, we need to demonstrate the reliability of these results.

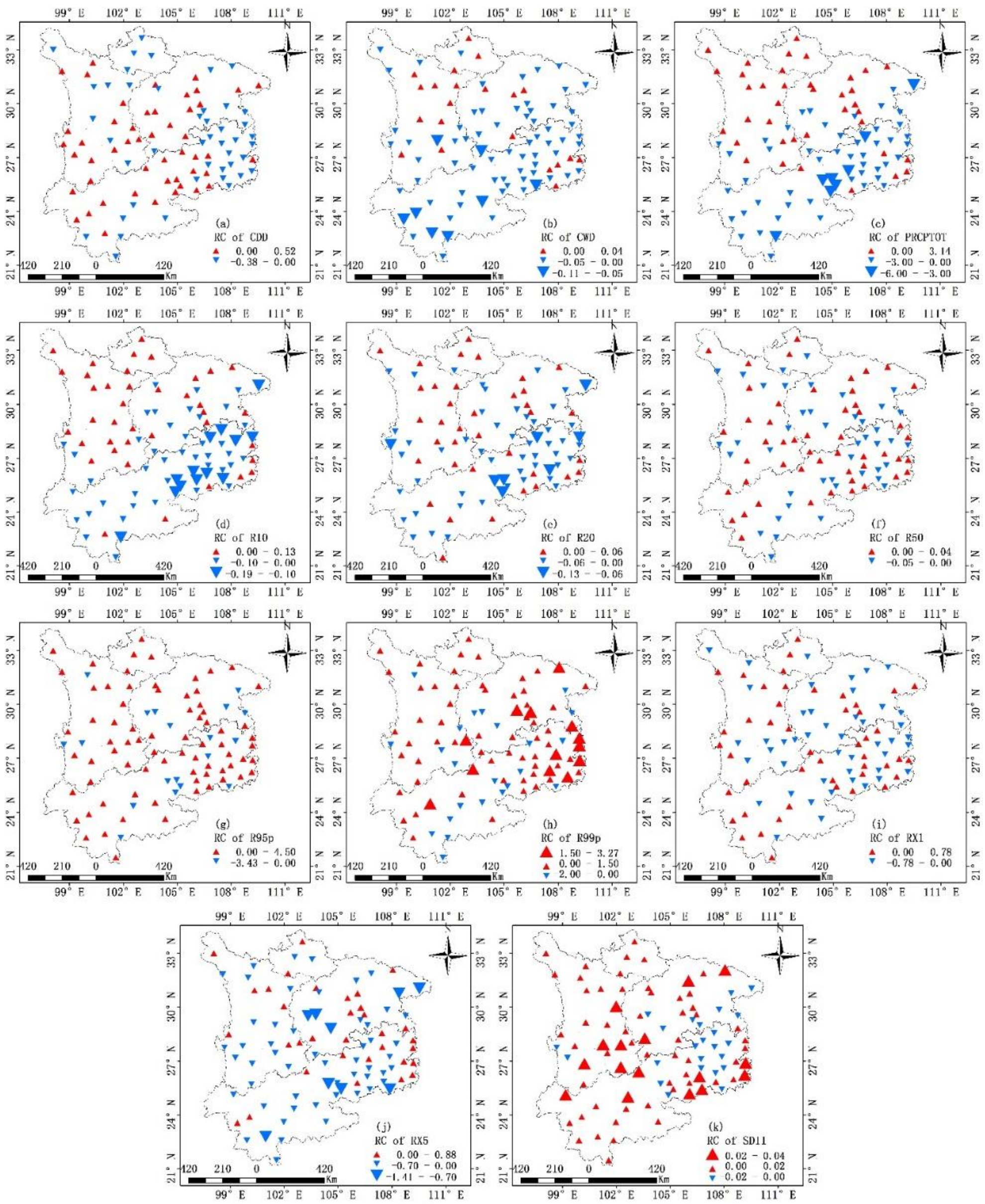

Figure 3. *Spatial variations in trends of 11 EPIs in Southwestern China from 1969 to 2020. (a) CDD (b) CWD (c) PRCPTOT (d) R10 (e) R20 (f) R50 (g) R95p (h) R99p (i) RX1 (j) RX5 (k) SDII*

Evaluation of the simulation performance of the models in CMIP6

Previous studies have shown that multimodal ensemble-based simulated values were similar to observed values (Zhao et al., 2014). Thus, in order to obtain MEM-9, nine models were combined into multimodel ensembles using model averaging. The Taylor diagram and skill score were used to compare the simulation performance of nine single models and MEM-9.

http://www.aloki.hu ● ISSN 1589 1623 (Print) ● ISSN 1785 0037 (Online)
DOI: http://dx.doi.org/10.15666/aeer/2106_53895414

Table 6. *The SACR (spatial average change rate) of 11 EPIs in Southwestern China and four different sub-regions from 1969 to 2020*

SACR	CDD (d/a)	CWD(d/a)	PRCPTOT (mm/a)	R10 (d/a)	R20 (d/a)	R50 (d/a)
Southwestern China	0.026	-0.018	-0.578	-0.028	-0.009	0.002
ZP (Zoige Plateau)	-0.132	-0.001	1.260	0.068	0.025	0.002
HMs (Hengduan Mountains)	0.073	-0.010	0.628	0.022	0.007	0.004
SB (Sichuan Basin)	0.037	-0.015	-0.094	-0.009	-0.005	0.002
YGP (Yunnan-Guizhou Plateau)	0.011	-0.026	-1.602	-0.071	-0.022	0.002
SACR	**R95p (mm/a)**	**R99p (mm/a)**	**RX1 (mm/a)**	**RX5 (mm/a)**	**SDII ((mm/d)/a)**	
Southwestern China	0.888	0.458	-0.021	-0.151	0.009	
ZP (Zoige Plateau)	0.682	0.287	0.153	-0.002	0.010	
HMs (Hengduan Mountains)	0.852	0.283	0.032	-0.150	0.010	
SB (Sichuan Basin)	0.968	0.526	-0.090	-0.171	0.007	
YGP (Yunnan-Guizhou Plateau)	0.882	0.525	-0.028	-0.154	0.008	

Figure 4 shows the Taylor diagram of 11 EPIs in Southwestern China based on simulated and observed data in the historical base period. REF represents the observed data. Results showed that the highest *R* and lowest *RMSE* were obtained using the CanESM5 model. Thus, this model displayed the best simulation performance for CDD and CWD. In addition, in this model, *STDR* was near 1.

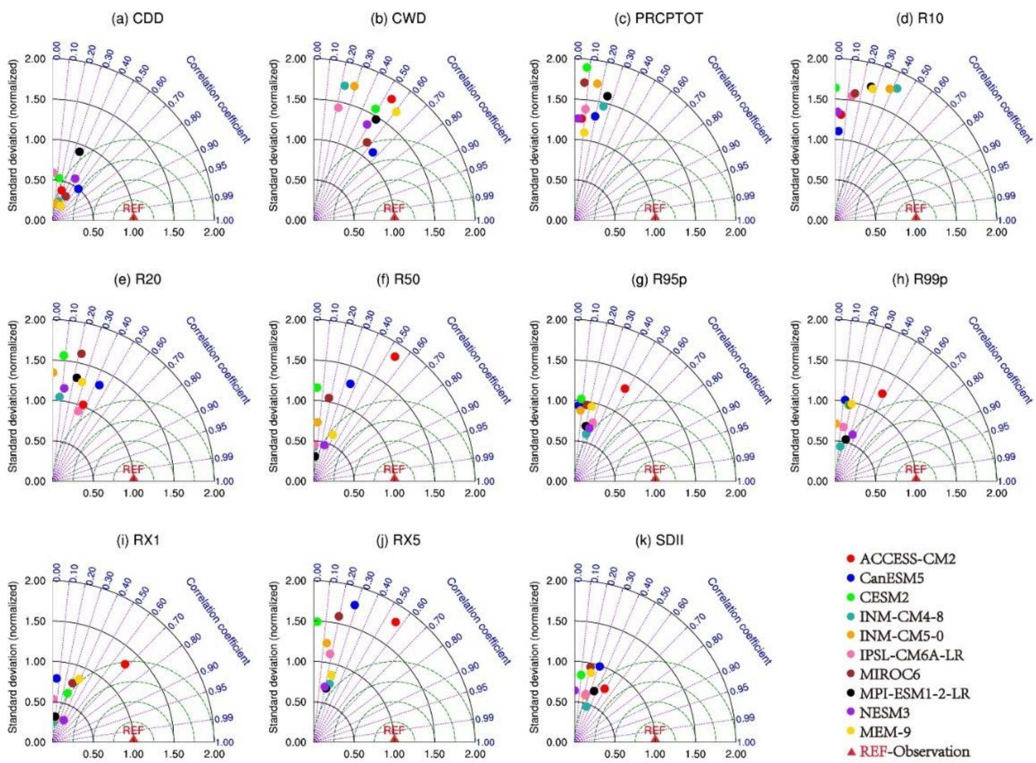

Figure 4. *Taylor diagram of 9 CMIP6 models and MEM-9 simulated fields relative to observed fields for 11 EPIs in the historical base period. (a) CDD (b) CWD (c) PRCPTOT (d) R10 (e) R20 (f) R50 (g) R95p (h) R99p (i) RX1 (j) RX5 (k) SDII*

http://www.aloki.hu ● ISSN 1589 1623 (Print) ● ISSN 1785 0037 (Online)
DOI: http://dx.doi.org/10.15666/aeer/2106_53895414

With respect to PRCPTOT and R10, the nine models and MEM-9 presented declined simulation performance with small *R* and large *RMSE*. However, when MEM-9, ACCESS-CM2, NESM3, and CanESM5 were used to simulate PRCPTOR, *STDR* showed values close to 1. Also, when ACCESS-CM2 and CanESM5 were applied in R10 simulation, *STDR* was close to 1. Regarding R20, ACCESS-CM2 resulted in *STDR* close to 1; also, CanESM5 displayed the highest *R*. Moreover, the two models displayed a small *RMSE*. As for the simulation of R50, the highest *R* and smallest *RMSE* were observed in ACCESS-CM2 and MEM-9, respectively. Furthermore, an *STDR* close to 1 was obtained when MEM-9 was used to simulate R95p, R99p, RX1, and RX5. In addition, the highest *R* corresponded to ACCESS-CM2. The nine models and MEM-9 had a low *R* when used to simulate SDII. ACCESS-CM2 had the highest *R* (0.5) and the lowest *RMSE*. CanESM5, MIROC6, and MEM-9 all presented an *STDR* close to 1. According to these data, although the simulated results of each index varied with different models, CanESM5, ACCESS-CM2, and MEM-9 had a relatively better simulation performance for the 11 EPIs studied in the present research.

Table 7 presents the *Ss* between 11 simulated and observed EPIs calculated with nine models and MEM-9 using *Equation (1)*. Results indicated that the *Ss* of the nine models and MEM-9 for all 11 EPIs were different. However, according to the average *S* of each model and MEM-9, the highest *Ss* were obtained with ACCESS-CM2, CanESM5 and MEM-9. These data were consistent with the results obtained through Taylor diagram analysis.

Table 7. *Skill scores (Ss) between simulated and observed EPIs for nine single models and MEM-9*

EPIs	ACCESS-CM2	CanESM5	CESM2	INM-CM4-8	INM-CM5-0	IPSL-CM6A-LR	MIROC6	MPI-ESM1-2-LR	NESM3	MEM-9
CDD	0.170	0.639	0.164	0.079	0.044	0.113	0.240	0.481	0.503	0.102
CWD	0.545	0.988	0.529	0.226	0.275	0.255	0.775	0.623	0.591	0.680
PRCPTOT	0.500	0.759	0.373	0.841	0.560	0.526	0.402	0.812	0.435	0.606
R10	0.278	0.276	0.193	0.720	0.654	0.331	0.349	0.462	0.243	0.488
R20	0.822	0.926	0.270	0.317	0.218	0.754	0.416	0.491	0.363	0.598
R50	0.704	0.548	0.197	0.094	0.203	0.112	0.338	0.067	0.280	0.508
R95p	0.932	0.257	0.287	0.384	0.285	0.548	0.378	0.382	0.472	0.468
R99p	0.958	0.335	0.397	0.192	0.197	0.320	0.429	0.350	0.559	0.448
RX1	0.929	0.149	0.279	0.037	0.063	0.090	0.349	0.056	0.166	0.447
RX5	0.720	0.336	0.161	0.392	0.261	0.322	0.279	0.320	0.301	0.404
SDII	0.928	0.606	0.284	0.357	0.344	0.365	0.429	0.592	0.170	0.455
Average S	0.680	0.529	0.285	0.331	0.282	0.340	0.399	0.421	0.371	0.473
Ranking	1	2	9	8	10	6	7	4	5	3

Future spatiotemporal variations of extreme precipitation events

Annual variation rates of 11 EPIs from 2021 to 2040

According to the Taylor diagram and skill score results of 11 EPIs obtained with nine models and MEM-9, CanESM5, ACCESS-CM2, and MEM-9 reported the best simulation performance. For this reason, they were selected to project future extreme precipitation events from 2021 to 2040 under the SSP2-4.5 scenario in Southwestern China. *Table 8* shows the projected annual change rates (ACRs) and annual average

http://www.aloki.hu ● ISSN 1589 1623 (Print) ● ISSN 1785 0037 (Online)
DOI: http://dx.doi.org/10.15666/aeer/2106_53895414

change rates (AACRs) of 11 EPIs. Except for AACRs of CDD and CWD that showed a decreasing trend, all other nine EPIs increased. In particular, PRCPTOT, R95p and R99p showed significant increasing trends of 5.48, 4.83 and 2.63, respectively. This indicated a reduction in the number of consecutive dry and wet days in the next 20 years in Southwestern China. However, it is expected that the amount of precipitation on wet days and the frequency and intensity of extreme precipitation will increase. In a word, extreme precipitation events will become more frequent.

Table 8. *Future projections of the ACRs (annual variation rates) and AACRs (annual average change rates) of 11 EPIs from 2021 to 2040 using different models under the SSP2-4.5 scenario*

EPIs	Models	ACRs	AACRs	EPIs	Models	ACRs	AACRs
CDD	MEM-9 CanESM5 ACCESS-CM2	-0.01 -0.42 0.11	-0.11	R95p	MEM-9 CanESM5 ACCESS-CM2	3.79 5.31 5.39	4.83
CWD	MEM-9 CanESM5 ACCESS-CM2	-0.56 0.06 -0.03	-0.18	R99p	MEM-9 CanESM5 ACCESS-CM2	2.44 2.92 2.54	2.63
PRCPTOT	MEM-9 CanESM5 ACCESS-CM2	3.13 5.81 7.48	5.48	RX1	MEM-9 CanESM5 ACCESS-CM2	0.13 0.49 0.46	0.36
R10	MEM-9 CanESM5 ACCESS-CM2	0.18 0.09 0.14	0.14	RX5	MEM-9 CanESM5 ACCESS-CM2	0.35 0.72 1.57	0.88
R20	MEM-9 CanESM5 ACCESS-CM2	0.09 0.08 0.15	0.11	SDII	MEM-9 CanESM5 ACCESS-CM2	0.01 0.01 0.02	0.01
R50	MEM-9 CanESM5 ACCESS-CM2	0.00 0.04 0.04	0.03				

As for the projection of ACRs of 11 EPIs using the two models and MEM-9, the ACR of CDD projected by ACCESS-CM2 was 0.11%, indicating an increasing trend. However, projections using MEM-9 and CanESM5 indicated a decreasing trend, as the ACR of CDD were -0.01% and -0.42%, respectively. The ACR of CWD projected by CanESM5 was 0.06%, indicating an increasing trend. Projections using ACCESS-CM2, and MEM-9 indicated a decreasing trend, and the decreasing rates were -0.03% and -0.56%, respectively. The projected range of PRCPTOT using the two models and MEM-9 was [3.31%, 7.84%]. The smallest and highest projected values were obtained with MEM-9 and ACCESS-CM2, correspondingly. The projected ranges of R10, R20, and R50 were [0.09%, 0.18%], [0.08%, 0.15%], and [0.00%, 0.04%], in that order. The projected R95p and R99p ranges were [3.79%, 5.39%] and [2.44%, 2.92%], respectively. In addition, when different models were used, the simulated values were alike. The projected RX1, RX5, and SDII ranges were [0.13%, 0.49%], [0.35%, 1.57%], and [0.01%, 0.02%], correspondingly. Also, the projected values were smaller with MEM-9 and larger with ACCESS-CM2. In general, the smallest and highest values obtained with the two models and MEM-9 corresponded to ACRs of EPIs projected with MEM-9, and those obtained with ACCESS-CM2, respectively.

http://www.aloki.hu ● ISSN 1589 1623 (Print) ● ISSN 1785 0037 (Online)
DOI: http://dx.doi.org/10.15666/aeer/2106_53895414

Temporal variation trends

Among the 11 EPIs, PRCPTOT, RX5, R99p, and R20 correspond to persistent index, intensity index, relative index, and absolute index, respectively. They represent the persistence and intensity of extreme precipitation events. In order to reduce projection uncertainty and increase accuracy and because of limited space, we applied the CanESM5, ACCESS-CM2, and MEM-9 to project the spatiotemporal variation trends of these four indices representing the extreme precipitation events from 2021 to 2040 under the SSP2-4.5 scenario. *Figure 5* shows the projected temporal variation trends in the next 20 years.

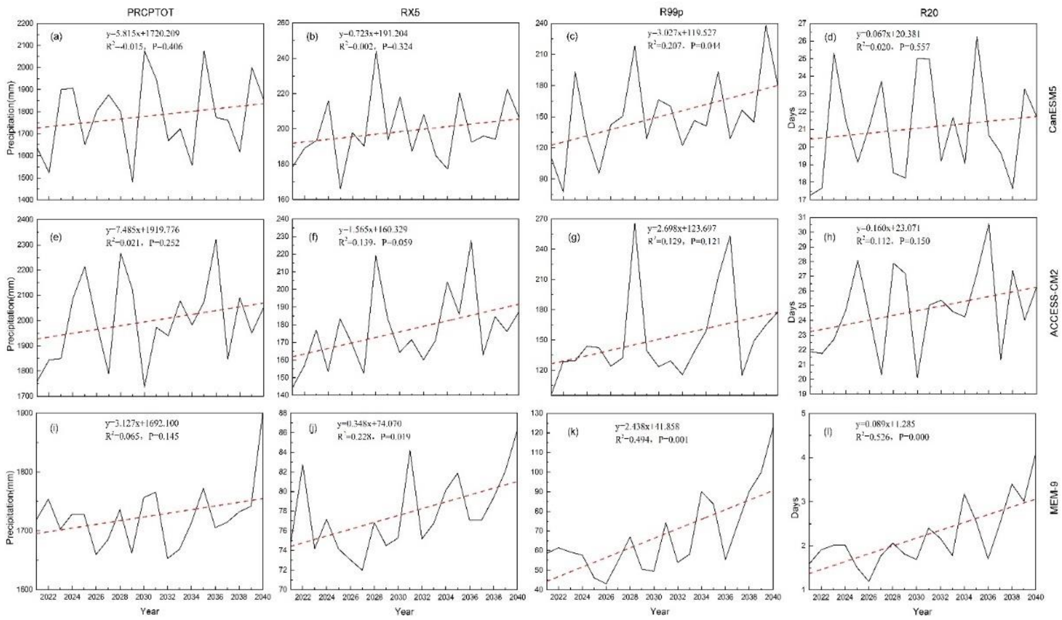

Figure 5. *Projections of temporal change trends of 4 EPIs in the next 20 years using different models under the SSP2-4.5 scenario. (a) CanESM5-PRCPTOT (b) CanESM5-RX5 (c) CanESM5-R99p (d) CanESM5-R20 (e) ACCESS-CM2-PRCPTOT (f) ACCESS-CM2-RX5 (g) ACCESS-CM2-R99p (h) ACCESS-CM2-R20 (i) MEM-9-PRCPTOT (j) MEM-9-RX5 (k) MEM-9-R99p (l) MEM-9-R20*

The four EPIs of PRCPTOT, RX5, R99p and R20 projected by the two models and MEM-9 generally showed an increasing trend from 2021 to 2040. The variation amplitude of PRCPTOT projected by CanESM5 was 1,481-2,076 mm, with the maximum peak occurring in 2030. The variation amplitude of RX5 was 160-250 mm, with the highest value in 2028. The variation amplitude of R99p projected by CanESM5 was 78-238 mm, and the peak was observed in 2039. The variation amplitude of R20 was 17-26 d, with the highest value occurring in 2035. However, except for R99p, the fitted values of PRCPTOT, RX5, and R20 projected by CanESM5 were not significant at the 0.05 level. The variation amplitude of PRCPTOT projected by ACCESS-CM2 was 1,735-2,322 mm, and the extremum appeared in 2036. The variation amplitude of RX5 was 144-228 mm, with the highest point located in 2036. R99p projected by ACCESS-CM2 showed a variation amplitude of 96-266 mm, and the extremum appeared in 2028. Also, R20 displayed a variation amplitude of 20-31 d, with the highest point located in 2036. It was also found that the fitted value of RX5 was significant at the 0.1 level, and other three indices were not significant at the 0.05 level. Moreover, PRCPTOT

http://www.aloki.hu ● ISSN 1589 1623 (Print) ● ISSN 1785 0037 (Online)
DOI: http://dx.doi.org/10.15666/aeer/2106_53895414

projected by MEM-9 presented a variation amplitude of 1,653-1,902 mm, with the extremum occurring in 2040. Also, RX5 displayed a variation amplitude of 72-86 mm, and the highest point in 2040. R99p projected by MEM-9 showed a variation amplitude of 43-123 mm, with the extremum occurring in 2040. Also, R20 displayed a variation amplitude of 1.2-4.1 d, and the highest point in 2040. Except for PRCPTOT, the fitted values of other three indices were significant at the 0.05 level. Especially, R99p and R20 passed the significance level test of 0.01. According to these results, the PRCPTOT values projected by the two models and MEM-9 were not significant at the 0.05 level. The RX5 values projected by MEM-9 and ACCESS-CM2 were significant at the 0.1 and 0.05 level, respectively. The R99p values projected by CanESM5 and MEM-9 passed the significance level test of 0.05 and 0.01, respectively. The R20 values projected by MEM-9 passed the significance level test of 0.01. According to these results, the values projected by MEM-9 had the highest significance level. In addition, the four EPIs extremes are expected to occur around 2040. On the other hand, RX5, R99p, and R20 projected with MEM-9 increased significantly; however, the smallest projected values and variation amplitude were obtained. In other words, PRCPTOT is expected to insignificantly increase in Southwestern China in the next 20 years. However, the duration and intensity of extreme precipitation events are expected to significantly increase.

Spatial variation trends

Figure 6 shows the projected spatial variation of *RC* for 4 EPIs in 93 weather stations for the next 20 years. According to our results, the projected values of PRCPTOT, RX5 and R99p using CanESM5 decreased from the middle to the north and south. The projected values of R20 obtained with CanESM5 decreased from southeast to northwest. Regions with increasing PRCPTOT, RX5, and R99p corresponded to YGP and southern HMs. Regions with increasing R20 corresponded to northeastern YGP. The values of PRCPTOT, RX5, R99p, and R20 projected by ACCESS-CM2 and MEM-9 generally showed an increasing trend. Especially, the most significant increase of 4 EPIs in ACCESS-CM2 was observed in eastern YGP. The projected values of R20 using ACCESS-CM2 presented a significant increase in HMs and western YGP. The values of 4 EPIs projected using MEM-9 showed a decrease in SB. Moreover, the SACRs projected by MEM-9 were much smaller than those obtained with the other two models. As previously shown, PRCPTOT, RX5, R99p, and R20 are expected to generally increase across the sub-regions in Southwestern China in the next 20 years. Regions with a high increase in PRCPTOT projected using the two models and MEM-9 were mainly found in YGP and southern HMs. These regions may experience a significant rise in total wet-day precipitation and precipitation persistence in the future. However, the regions that involved a high increase in RX5 varied considerably across the two models and MEM-9. Regions with a high increase in R99p and R20 projected using the two models and MEM-9 were mainly found in eastern YGP. These regions may experience a significant increase in rainfall intensity and extreme precipitation events in the future. Also, the regions that showed a decrease in 4 EPIs projected using the two models and MEM-9 were mainly found in SB.

http://www.aloki.hu ● ISSN 1589 1623 (Print) ● ISSN 1785 0037 (Online)
DOI: http://dx.doi.org/10.15666/aeer/2106_53895414

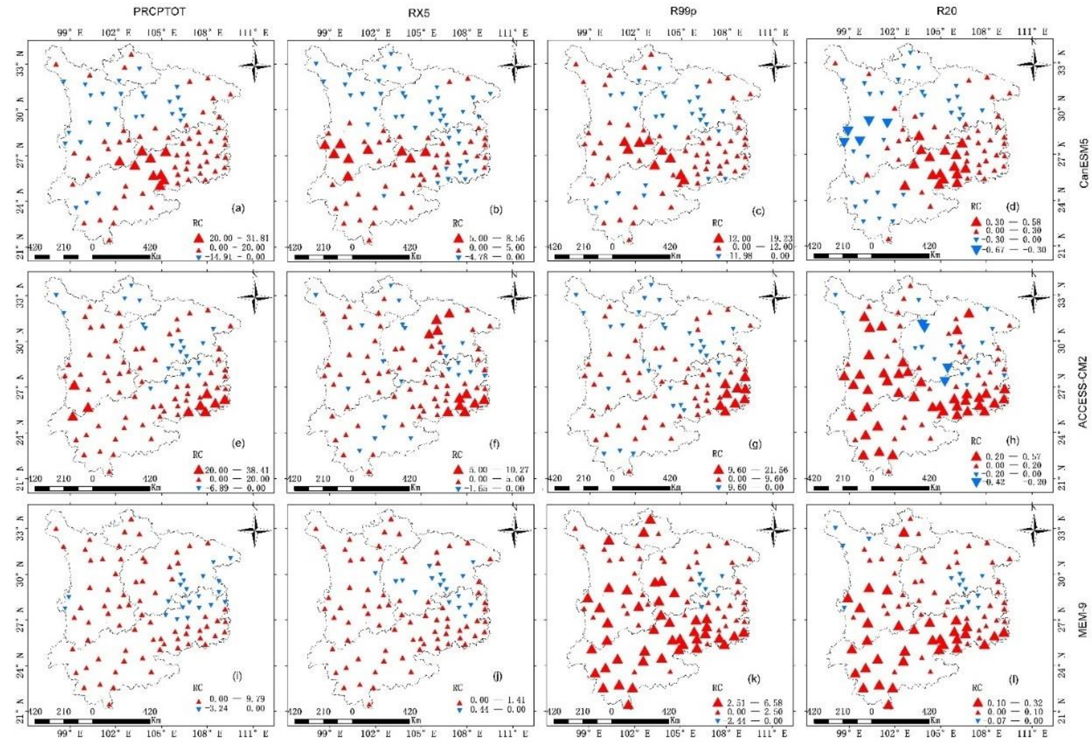

***Figure 6.** Projections of the spatial variation trends of 4 EPIs in the next 20 years using different models under the SSP2-4.5 scenario. (a) CanESM5-PRCPTOT (b) CanESM5-RX5 (c) CanESM5-R99p (d) CanESM5-R20 (e) ACCESS-CM2-PRCPTOT (f) ACCESS-CM2-RX5 (g) ACCESS-CM2-R99p (h) ACCESS-CM2-R20 (i) MEM-9-PRCPTOT (j) MEM-9-RX5 (k) MEM-9-R99p (l) MEM-9-R20*

Variation trends in the four sub-regions

Table 9 shows the four projected EPIs average values for different sub-regions of Southwestern China from 2021 to 2040 under the SSP2-4.5 scenario. These values were obtained using the two models and MEM-9. The averages of four EPIs projected by CanESM5 in different sub-regions showed that the highest and lowest PRCPTOT and RX5 corresponded to HMs and SB, respectively. However, HMs and YGB showed the highest and lowest R99p and R20, correspondingly. The projections using ACCESS-CM2 showed that the largest and smallest PRCPTOT values were observed in HMs and SB, in that order. The largest and smallest RX5 and R20 values were observed in YGP and ZP, correspondingly; however, the largest and smallest R99p values were observed in YGP and HMs, respectively. In addition, the projections using MEM-9 indicated that the highest and lowest PRCPTOT corresponded to ZP and SB, in that order; However, the highest and lowest RX5, R99p and R20 corresponded to YGB and SB. The PRCPTOT ranges projected using the two models and MEM-9 for the four sub-regions were as follows: [1993.54-2066.03] mm for ZP, [1886.67-2250.60] mm for HMs, [1501.97-1812.37] mm for SB, and [1615.53-2054.22] mm for YGP. The projected PRCPTOT displayed the highest average value in HMs and the lowest average in SB. The RX5 ranges projected using the two models and MEM-9 for the four sub-regions were: [80.22-215.45] mm for ZP, [81.66-264.53] mm for HMs, [61.52-181.75] mm for SB, and [84.00-212.74] mm for YGP. Data indicated that the lowest and highest projected average RX5 were observed in ZP and YGP. According to our results, the R99p ranges

http://www.aloki.hu ● ISSN 1589 1623 (Print) ● ISSN 1785 0037 (Online)
DOI: http://dx.doi.org/10.15666/aeer/2106_53895414

projected using the two models and MEM-9 were: [70.97-150.90] mm for ZP, [66.34-188.60] mm for HMs, [61.18-158.66] mm for SB, and [70.97-183.25] mm for YGP. Also, the largest and smallest average R99p corresponded to YGP and ZP, respectively. On the other hand, the projected R20 ranges obtained with the two models and MEM-9 were: [1.725-30.83] d for ZP, [2.69-31.39] d for HMs, [0.87-22.35] d for SB, and [2.78-27.56] d for YGP. The highest and smallest average R20 values were observed in HMs and SB, correspondingly. It was also determined that the smallest average EPIs were obtained using MEM-9. Moreover, the RX5, R99p, and R20 values obtained with MEM-9 displayed larger differences as compared to the values calculated using the other two models. These projections showed that in the next 20 years, HMs is expected to have the highest PRCPTOT and SB the lowest PRCPTOT. In addition, projections indicated that from 2021 to 2040, the highest and lowest RX5 and R99p will be observed in YGB and ZP, respectively. However, no differences will be observed in R20 in the four sub-regions. These results also indicate that in the next 20 years, the most extreme precipitation events with the longest duration and highest intensity are expected to occur in HMs and YGB. Projections showed that the opposite will be observed in SB and ZP.

Table 9. *Future projections (2021-2040) for average values of the 4 EPIs in different sub-regions obtained with two models and MEM-9 under the SSP2-4.5 scenario*

EPIs	**Models** / **Sub-regions**	**CanESM5**	**ACCESS-CM2**	**MEM-9**	**Average values of models**
PRCPTOT (mm)	ZP (Zoige Plateau)	2004.48	1993.54	2066.03	2021.35
	HMs (Hengduan Mountains)	2250.60	2070.11	1886.67	2069.13
	SB (Sichuan Basin)	1594.96	1812.37	1501.97	1636.43
	YGP (Yunnan-Guizhou Plateau)	1615.53	2054.22	1729.61	1799.79
RX5 (mm)	ZP (Zoige Plateau)	215.45	91.18	80.22	128.95
	HMs (Hengduan Mountains)	264.53	112.82	81.66	153.00
	SB (Sichuan Basin)	170.40	181.75	61.52	137.89
	YGP (Yunnan-Guizhou Plateau)	178.44	212.74	84.00	158.39
R99p (mm)	ZP (Zoige Plateau)	150.90	89.48	70.96	103.78
	HMs (Hengduan Mountains)	188.60	88.32	66.34	114.42
	SB (Sichuan Basin)	140.23	158.66	61.18	120.02
	YGP (Yunnan-Guizhou Plateau)	135.30	183.25	70.97	129.84
R20 (d)	ZP (Zoige Plateau)	30.83	17.93	1.725	16.83
	HMs (Hengduan Mountains)	31.39	22.54	2.59	18.84
	SB (Sichuan Basin)	19.23	22.35	0.87	14.15
	YGP (Yunnan-Guizhou Plateau)	15.95	27.56	2.78	15.43

According to the data presented in *Table 5*, when the four EPIs averages of the historical period (1969-2020) were compared with the EPIs obtained with the two models and MEM-9, it was found that in the next 20 years under the SSP2-4.5 scenario: PRCPTOT showed an increasing trend in the four subregions, with the largest increase in ZP and the smallest in SB; RX5 also showed an increasing trend in three sub-regions and a decreasing trend SB. In this case, the highest and lowest RX5 increase was observed in ZP and YGP, respectively; R99p tended to increase in the four sub-regions. Herein, the

http://www.aloki.hu ● ISSN 1589 1623 (Print) ● ISSN 1785 0037 (Online)
DOI: http://dx.doi.org/10.15666/aeer/2106_53895414

largest and smallest increment corresponded to HMs and SB, respectively. In addition, R20 showed a rising trend in ZP and HMs, and a decreasing trend in SB and YGP. Thus, compared to the historical period, in the next 20 years the most significant amplitude increase will be observed in ZP and HMs, where the most elevated number of wet-days will occur along with the highest persistence and intensity of extreme precipitation events. Next in order will be YGP. In addition, precipitation will increase in SB with slight changes in the intensity of extreme precipitation events.

Discussion

In recent years, the interest to study extreme precipitation events has increased. In this context, several achievements have been made (Barlow et al., 2019; Mahbod et al., 2020; Mondal et al., 2020; Sourav et al., 2021; Blanka et al., 2021; Deepanshu et al., 2022; Mohammad et al., 2022; Hidalgo et al., 2022; Antokhina et al., 2023; Corona et al., 2023). The distribution of extreme precipitation events and the evolutionary trend vary due to regional differences. Southwestern China is particularly susceptible to the influence of monsoons and is widely known for its complex topography. This region depends on the joint action of several factors, including climate and topography. This has resulted in marked spatial and temporal variations in extreme precipitation events within the region. We have analyzed the spatial and temporal variations of extreme precipitation events in Southwestern China from 1969 to 2020. Although precipitation on wet days and the number of consecutive days with rainfall showed interdecadal decrease, the frequency of strong precipitation and the precipitation intensity increased. Both the intensity and frequency of extreme precipitation events increased in Southwestern China. However, substantial differences in extreme precipitation events within Southwestern China were observed. The number of consecutive dry days generally increased at each station, while the number of consecutive days with rainfalls decreased. The frequency of strong precipitation and the amount of extreme strong precipitation insignificantly decreased from southeast to northwest. We determined that the spatial and temporal variations of these indices in historical periods were consistent with those reported by Yuan et al. (2014), Liu et al. (2014), Luo et al. (2015), and Lu et al. (2017). However, variation amplitudes were slightly different, depending on the dataset used and the time scale. Previous studies analyzes spatial variations considering administrative divisions. In the present research, we selected topographic and meteorological conditions as criteria to highlight regional contrasts. Different precipitation features were found in the four sub-regions. Extreme precipitation events are greatly influenced by human activities, and the frequency is higher in more densely populated regions. This is especially true in Southwestern China, which is known for its considerable vulnerability to climate change. This conclusion agreed with those published by Li (2018) and Zhao et al. (2019), who also studied Southwestern China.

Since the implementation of CMIP, future projections of extreme climate indices have generally shown that climate models have significantly better simulation performance for extreme temperature indices than EPIs, and present greater uncertainty during EPIs simulations and projections. Overall, CMIP6 is better than CMIP5 on simulation performance. Zhu et al. (2020) indicated that CMIP6 models showed improvements in the simulation of climate indices over China as compared to CMIP5. This was particularly true for precipitation indices related to climatological pattern and interannual variations, except for CDD. The areal-mean bias of total precipitation dropped from 127% (CMIP5

http://www.aloki.hu ● ISSN 1589 1623 (Print) ● ISSN 1785 0037 (Online)
DOI: http://dx.doi.org/10.15666/aeer/2106_53895414

multi-model ensemble mean) to 79% (CMIP6 multi-model ensemble mean). Moreover, Ai et al. (2021) reported that the CMIP6 models were generally able to capture mean climate extremes and trends. The CMIP6 multimodel median ensemble (MME) typically outperformed the individual models in simulating spring climate extremes. However, in terms of the model performance metrics, almost no models showed better performance in reference to all indices compared to the observations. Xu et al. (2022) assessed model capabilities when simulating precipitation extremes across China. For this purpose, they used 30 CMIP5 and 36 CMIP6 models. Their results indicated that CMIP6 models generally exhibited superior skill in simulating the EPIs over China. In addition, smaller variabilities were obtained with CMIP6. We plotted the Taylor diagram and calculated skill scores to assess the simulation performance of the nine models and MEM-9 in the historical base period before making the projections of 11 EPIs for the next 20 years. We found that, although the average simulation performance of the multimodel ensemble was better than that obtained using individual models, the simulation performance of the nine single models and MEM-9 varied considerably for different EPIs. This result agreed with the findings previously mentioned. Thus, in order to improve the projection reliability and to reduce uncertainty, we selected ACCESS-CM2, CanESM5, and MEM-9 for further projections.

To the best of our knowledge, many projections of extreme precipitation events have been performed on the global and large regional scales. However, few projection studies have focused on the small regional scale, especially in Southwestern China. Taking into account existing projections of future extreme precipitation events in Southwestern China, IPCC AR6 has pointed out that strong precipitation events in 19 regions, including the Qinghai-Tibet Plateau and East Asia, will increase in both intensity and frequency (IPCC, 2021; Zhou and Qian, 2021). Our findings were consistent with those reported by AR6.

In a similar study, Xiang et al. (2021) assessed the capabilities of CMIP6 models to project extreme precipitations in the major regions of China. They reported significant differences in the simulation of EPIs using different GCMs. The bias-corrected EC-Earth3 was used for the projection of the average annual precipitation, the number of very heavy rainfall days above 50 mm (R50), the fraction of total precipitation above the 95th percentile (R95), and the contribution rate of extreme precipitation (R95T) in the future. Their results indicated that these four EPIs displayed an increasing trend under the SSP2-4.5 scenario in Southwestern China from 2021 to 2100. The four EPIs obtained under the SSP2-4.5 scenario showed differences in their average values when the historical period (1979 to 2014) was compared with future projections. Most of the indices showed an increasing trend in Southwestern China. Some parts of Yunnan were the exception, as it showed a reduction in the average annual precipitation. These results were consistent with those obtained herein for the ACRs of PRCPTOT, R20, and R95p, as well as the spatial and temporal variations of PRCPTOT. However, the projected increasing amplitudes varied due to differences in the models used and the time periods covered. The two models and MEM-9 selected according to the Taylor diagram and skill score results were further used to project future spatial variation of PRCPTOT. Except for the CanESM5-based projection that indicated a decreasing trend in the annual average precipitation in some parts of Yunnan, the projections using ACCESS-CM2, and MEM-9 indicated an increasing trend in the annual average precipitation in Yunnan. Furthermore, other parts of Southwestern China did not show an increase in the annual average precipitation. The regions with a high amplitude increase of PRCPTOT projected by the two models and MEM-9 were mainly located in the central and eastern parts of YGP and

http://www.aloki.hu ● ISSN 1589 1623 (Print) ● ISSN 1785 0037 (Online)
DOI: http://dx.doi.org/10.15666/aeer/2106_53895414

the southern part of HMs. This conclusion diverged from that elaborated by Xiang et al. (2021). One of the highlights of the present study was that the ACRs of 11 EPIs were projected for the next 20 years. Hu et al. (2020b) projected future changes in consecutive climate events in Southwestern China using the RegCM4.0 and BCC_CSM1.1 data under the RCP4.5 scenario from 2025 to 2055. According to their data, a weak increasing trend in GCWD and GCDD was projected in this region. In the present research, ACRs of CDD and CWD were projected from 2021 to 2040. Except for a weak increasing trend in CDD as projected by ACCESS-CM2, a weak decreasing trend was projected using MEM-9 and CanESM5. As for CWD projection, except for a weak increasing trend using CanESM5, a weak decreasing trend was obtained with MEM-9 and ACCESS-CM2. AACRs of these two indices showed a weak decreasing trend. This result diverged from that reported by Hu et al. (2020b). These analyses suggested a considerable uncertainty in the projection of the same EPIs in Southwestern China due to the joint action of several factors, including model-related factors (e.g., physical mechanism, structural principle, climate forcing, model resolution, and emission scenario design) and external conditions (complex topography, ecological environment changes, and socioeconomic development) (Zhao et al., 2019).

Since existing studies have shown that the signal-to-noise ratio under the high emission scenario is generally larger than that under the low emission scenario, and the variation trend of EPIs in major regions of China has a small difference among different scenarios in the near future, we selected the SSP2-4.5 scenario to obtain projections in the near future (2021-2040). This scenario is more in line with China's national conditions. However, it is a relatively short future period. In the projection of future spatiotemporal variation trend of extreme precipitation events, only 4 representative indices of 11 EPIs were selected for analysis due to space limitation. Considering the spatial resolution of the study area, we performed data processing by statistically downscaling the CMIP6 models. However, this method may increase model projection uncertainty. These deficiencies may be addressed by adding a variety of scenarios, increasing the projection period, using the CMIP6 multi-model ensemble with different weights, bias correction, super-ensemble simulation techniques, use of the regional climate model, and a variety of statistical and dynamic downscaling methods. These data processing methodologies are expected to enhance projection reliability, and they will be further developed and improved as part of future research.

Conclusions

In the present investigation, we determined spatiotemporal variations of historical extreme precipitation events from 1969 to 2020 and the spatiotemporal variation trend of future extreme precipitation events from 2021 to 2040 under the SSP2-4.5 scenario in Southwestern China. According to our results, we formulated the following conclusions:

(1) In general, Southwestern China showed a continuous reduction in precipitation days; however, increasing precipitation intensity and increasing extreme precipitation events were observed from 1969 to 2020. The four sub-regions also showed different extreme precipitation degrees. Commonly, extreme precipitation events are substantially influenced by human activities. The precipitation is usually more intense in regions that are densely populated and with higher urbanization rates (SB and YGP). Also, extreme precipitation events occur at a higher frequency and a higher intensity in such regions. As shown by the distribution of SACR at 93 stations in 52 years, CDD increased and CWD

http://www.aloki.hu ● ISSN 1589 1623 (Print) ● ISSN 1785 0037 (Online)
DOI: http://dx.doi.org/10.15666/aeer/2106_53895414

decreased at different stations in Southwestern China. PRCPTOT decreased from northwest to southeast. However, extreme precipitation events occurred more frequently over time. The most dramatic increase in the frequency of extreme precipitation events occurred in HMs.

(2) Taylor diagram and skill score results showed that ACCESS-CM2, CanESM5 and MEM-9 had a relatively better simulation performance for the 11 EPIs. The overall analysis of the ACRs of 11 EPIs in Southwestern China from 2021 to 2040 under the SSP2-4.5 scenario showed that the number of consecutive dry and wet days will likely decrease in the next 20 years. However, the amount of precipitation on wet days, the frequency and intensity of extreme precipitation will likely increase. In summary, extreme precipitation events will be more common. The ACRs of EPIs projected by the MEM-9 were smaller among the ACCESS-CM2, CanESM5, and MEM-9, while those obtained with ACCESS-CM2 were larger.

(3) The results of temporal change trends of the 4 EPIs representing extreme precipitation events indicated that PRCPTOT will insignificantly increase in Southwestern China in the next 20 years, while RX5, R99p, and R20 will significantly increase. The results of spatial variation trends indicated that 4 EPIs will increase across the sub-regions in Southwestern China in the next 20 years. Regions with a high increase in PRCPTOT projected using the two models and MEM-9 were mainly found in YGP and southern HMs. However, the regions with a high increase in RX5 varied considerably across the two models and MEM-9. Regions with a high increase in R99p and R20 were mainly found in eastern YGP.

(4) According to the projected averages of the 4 sub-regional EPIs, it is expected that events displaying the longest duration, highest intensity, and most extreme precipitation will occur in HMs and YGB. However, the opposite is likely to occur in SB and ZP in the next 20 years under the SSP2-4.5 scenario. Comparing the 4 EPIs mean values of 1969-2020, we found that the most significant amplitude increase will occur in ZP and HMs. These regions are expected to present the most intense precipitation in wet-days, and the highest persistence and intensity of extreme precipitation events. After ZP and HMs, YGP will follow. Moreover, persistence of precipitation will increase in SB and the intensity of extreme precipitation will display little changes in the two periods.

Acknowledgments. This work was jointly funded by the Key Research and Development (R&D) Project in Department of Science and Technology of Yunnan Province (202203AC100005, 202203AC100006) and Drought Meteorological Science Research Fund of the China Meteorological Administration (IAM202201). The authors thank the modelling groups, the Coupled Model Inter-comparison Project Phase 6 of the World Climate Research Program (WCRP) (https://esgf-index1.ceda.ac.uk/projects/cmip6-ceda/) for their roles in making available the nine-model data set.

REFERENCES

[1] Agel, L., Barlow, M. (2020): How well do CMIP6 historical runs match observed Northeast U.S. precipitation and extreme precipitation–related circulation? – Journal of Climate 33: 9835-9848.

[2] Ai, Y. W., Chen, H. P., Sun, J. Q. (2021): Model assessments and future projections of spring climate extremes in China based on CMIP6 models. – International Journal of Climatology 42(9): 4601-4620.

http://www.aloki.hu ● ISSN 1589 1623 (Print) ● ISSN 1785 0037 (Online)
DOI: http://dx.doi.org/10.15666/aeer/2106_53895414

[3] Akinsanola, A. A., Ongoma, V., Kooperman, G. J. (2021): Evaluation of CMIP6 models in simulating the statistics of extreme precipitation over Eastern Africa. – Atmospheric Research 254: 105509.
[4] Allen, M. R., Ingram, W. J. (2012): Constraints on future changes in climate and the hydrologic cycle. – Nature 489(7417): 590-598.
[5] Antokhina, O., Antokhin, P., Gochakov, A., Zbirannik, A., Gazimov, T. (2023): Atmospheric circulation patterns associated with extreme precipitation events in eastern Siberia and Mongolia. – Atmosphere 14: 480.
[6] Barlow, M., Gutowski, W. J., Gyakum, R. J., Katz, R. W., Lim, Y. K., Schumacher, R. S., Wehner, M. F., Agel, L., Bosilovich, M., Collow, A., Gershunov, A., Grotjahn, R., Leung, R., Milrad, S., Min, S. K. (2019): North American extreme precipitation events and related large-scale meteorological patterns: a review of statistical methods, dynamics, modelling, and trends. – Climate Dynamics 53(11): 6835-6875.
[7] Blanka, G., Miloslav, M., Blanka, G. M. M. (2021): Predictability of moisture flux anomalies indicating central European extreme precipitation events. – Quarterly Journal of the Royal Meteorological Society 147(739): 3335-3348.
[8] Chen, H. P., Sun, J. Q., Lin, W. Q., Xu, H. W. (2020): Comparison of CMIP6 and CMIP5 models in simulating climate extremes. – Science Bulletin 65: 1415-1418.
[9] Chen, Z. F., Li, X. H., Wang, L. (2022): Spatiotemporal changes of extreme temperatures in the past 49 years and their relationship with the ENSO in Southwestern China. – Applied Ecology of Environmental Research 20(2): 1113-1138.
[10] Cheng, X. R. (2019): Prediction of spatio-temporal characteristics of temperature and precipitation over the upstream of Yangtze River Basin based on CMIP5 mode. – Water Resources and Power 37(1): 13-16.
[11] China Meteorological Administration Climate Change Centre (2021): Blue Book on Climate Change in China Beijing. – Science Press.
[12] Corona, C. R., Ge, S. M., Anderson, S. P. (2023): Water-table response to extreme precipitation events. – Journal of Hydrology 618: 129140.
[13] Deepanshu, A., Raju, A., Shukla, K. K., Rohit, C., Ravi, K. K. (2022): Monsoon precipitation characteristics and extreme precipitation events over Northwest India using Indian high resolution regional reanalysis. – Atmospheric Research 267: 105993.
[14] Ding, W. R. (2014): Spatial and temporal variability of the extreme daily precipitation in Southwest China. – Resources and environment in the Yangtze Basin 23(7): 1071-1079.
[15] Dong, T. Y., Dong, W. J. (2021): Evaluation of extreme precipitation over Asia in CMIP6 models. – Climate Dynamics 57: 1751-1769.
[16] Gupta, V., Singh, V., Jain, M. K. (2020): Assessment of precipitation extremes in India during the 21st century under SSP1-1.9 mitigation scenarios of CMIP6 GCMs. – Journal of Hydrology 590: 125422.
[17] Hidalgo, H. G., Alfaro, E. J., Valverde, K. T., Juan, B. (2022): Probability of induced extreme precipitation events in central America due to tropical cyclone positions in the surrounding oceans. – Natural Hazards 116(3): 2917-2933.
[18] Hu, Z. H., Li, Y. H., Hu, Y. W., Wang, Y. (2020a): Prediction of future precipitation in Southwest China by CMIP5 and RegCM4.0. – Mid-low Latitude Mountain Meteorology 44(5): 19-25.
[19] Hu, Z. H., Li, Y. H., Hu, Y. W., Wang, Y. (2020b): Prediction of future change of persistent climate event in Southwest China. – Journal of the Meteorological Sciences 40(6): 829-837.
[20] IPCC. (2021): Climate change 2021: The physical science basis [M/OL]. – [2021-08-01]. https://www.ipcc.ch/report/ar6/wgl/downloads/report/IPCC_AR6_WGI_Full_Report.pdf.
[21] Jiang, T., Lv, Y. R., Huang, J. L., Wang, Y. J., Su, B. D., Tao, H. (2020): New scenarios of CMIP6 Model (SSP-RCP) and its application in the Huaihe River Basin. – Advances in Met. S&T 10(5): 102-109.

http://www.aloki.hu ● ISSN 1589 1623 (Print) ● ISSN 1785 0037 (Online)
DOI: http://dx.doi.org/10.15666/aeer/2106_53895414

[22] Jiang, W. H., Chen, H. P. (2021): Assessment and projection of changes in temperature extremes over the mid-high latitudes of Asia based on CMIP6 models. – Trans. Atmos. Sci. 44(4): 592-603.
[23] Klutse, N. A. B., Quagraine, K. A., Nkrumah, F., Quagraine, K. T., Berkoh-Oforiwaa, R., Dzrobi, J. F., Sylla, M. B. (2021): The climatic analysis of summer monsoon extreme precipitation events over West Africa in CMIP6 simulations. – Earth Systems and Environment 5: 25-41.
[24] Li, W. (2018): Detection of anthropogenic signal and projection in extreme precipitation changes over China. – Nanjing University of Information Science & Technology, Nanjing.
[25] Li, X. H., Chen, Z. F., Wang, L. (2020): Analysis of the spatiotemporal variation characteristics of main extreme climate indices in Sichuan Province of China from 1968 to 2017. – Applied Ecology of Environmental Research 18(2): 3211-3242.
[26] Li, J., Huo, R., Chen, H., Zhao, Y., Zhao, T. (2021): Comparative assessment and future prediction using CMIP6 and CMIP5 for annual precipitation and extreme precipitation simulation. – Front. Earth Sci. 9: 687976.
[27] Liu, L., Xu, Z. X. (2014): Spatiotemporal distribution of the extreme climate indices in the five southwestern provinces of China. – Resources and Environment in the Yangtze Basin 23(2): 294-301.
[28] Lu, J. Y., Yan, J. P., Cao, Y. W. (2017): Spatial distribution characteristics of precipitation and flood index in Southwestern China during 1961-2015. – Resources and Environment in the Yangtze Basin 26(10): 1711-1720.
[29] Luo, Y., Fan, G. Z., Zhou, D. W., Hua, W., Li, J. J. (2015): Extreme precipitation trend of Southwest China in recent 41 years. – Journal of the Meteorological Sciences 35(5): 581-586.
[30] Mahbod, M., Rafiee, R. M. (2020): Trend analysis of extreme precipitation events across Iran using percentile indices. – International Journal of Climatology 41(2): 952-969.
[31] Mohammad, R. E., Akbar, R., Haniyeh, S., Luca, B., Mikołaj, P. (2022): Detecting characteristics of extreme precipitation events using regional and satellite-based precipitation gridded datasets over a region in Central Europe. – The Science of the total Environment 852: 158497.
[32] Mondal, S., Mishra, K. A., Leung, R. L. (2020): Spatiotemporal characteristics and propagation of summer extreme precipitation events over United States: A complex network analysis. – Geophysical Research Letters 47(15): 1-11.
[33] Peterson, T. C., Zhang, X. B., Brunet-India, M., Vazquez-Aguirre, J. L. (2008): Changes in North American extremes derived from daily weather data. – Journal of Geophysical Research 113: D07113.
[34] Scoccimarro, E., Gualdi, S. (2020): Heavy daily precipitation events in the CMIP6 worst-case scenario: Projected twenty-first-century changes. – Journal of Climate 33: 7631-7642.
[35] Sourav, M, Ashok, K. M (2021): Cascading effect of meteorological forcing on extreme precipitation events: Role of atmospheric rivers in southeastern US. – Journal of Hydrology 601: 126641.
[36] Srivastava, A., Grotjahn, R., Ullrich, P. A. (2020): Evaluation of historical CMIP6 model simulations of extreme precipitation over contiguous US regions. – Weather and Climate Extremes 29: 100268.
[37] Sun, F. Y. (2018): Drought and flood outlook for the Yangtze River Basin. – East China Normal University, Shanghai.
[38] Taylor, K. R. (2001): Summarizing multiple aspects of model performance in a single diagram. – Journal of Geophysical Research 106: 7183-7192.
[39] Wang, Y., Li, H. X., Wang, H. J., Sun, B., Chen, H. P. (2021): Evaluation of CMIP6 model simulations of extreme precipitation in China and comparison with CMIP5. – Acta Meteorologica Sinica 79(3): 369-386.
[40] Wentz, F. J., Ricciardulli, L., Hilburn, K., Mears, C. (2007): How much more rain will global warming bring? – Science 317(5835): 233-235.

http://www.aloki.hu ● ISSN 1589 1623 (Print) ● ISSN 1785 0037 (Online)
DOI: http://dx.doi.org/10.15666/aeer/2106_53895414

[41] Wu, D., Pei, Y. S., Zhao, Y., Xiao, W. H. (2012): Numerical simulations of climate change under IPCC A1B scenario in Southwestern China. – Progress in Geography 31(3): 275-284.
[42] Xiang, J. W., Zhang, L. P., Deng, Y., She, D. X., Zhang, Q. (2021): Projection and evaluation of extreme temperature and precipitation in major regions of China by CMIP6 models. – Engineering Journal of Wuhan University 54(1): 46-57+81.
[43] Xu, H. W., Chen, H. P., Wang, H. J. (2022): Future changes in precipitation extremes across China based on CMIP6 models. – International Journal of Climatology 42(1): 635-651.
[44] Xue, Y. T., Li, X. H., Wang, L., Xu, B. (2022): Spatial and temporal change characteristics of different grades of precipitation in summer in Southwestern China from 1976 to 2017. – Journal of Southwest University (Natural Science Edition) 44(2): 137-145.
[45] Yan, Z. T., Li, X. H., Liu, Z. T., Xu, J. A., Pan, Y. S. (2021): Risk change of rainstorm and flood disaster in four provinces and cities of Southwestern China under the background of climate warming. – Journal of Catastrophology 36(2): 200-207.
[46] Yang, X. L., Zhou, B. T., Xu, Y., Han, Z. Y. (2021): CMIP6 evaluation and projection of temperature and precipitation over China. – Adv. Atmos. Sci. 38(5): 817-830.
[47] Yuan, W. D., Zheng, J. K., Dong, K. (2014): Spatial and Temporal Variation in Extreme Precipitation Events in Southwestern China during 1962-2012. – Resources Science 36(4): 766-772.
[48] Zarrin, A., Dadashi-Roudbari, A. (2021): Projection of future extreme precipitation in Iran based on CMIP6 multi-model ensemble. – Theoretical and Applied Climatology 144: 643-660.
[49] Zhang, X., Yang, F. (2004): RClimDex 1.1. – http://etccdi.pacificclimate.org/software.shtml.
[50] Zhang, W. L., Zhang, J. Y., Fan, G. Z. (2015): Evaluation and projection of dry- and wet-season precipitation in Southwestern China using CMIP5 models. – Chinese Journal of Atmospheric Science 39(3): 559-570.
[51] Zhang, C., Cheng, J., Xu, R. (2016): Comparative Analysis on Mean Amounts of Precipitation and its Changes during 21st Century in Southwest China Predicted by CMIP5 Multi-modes. – Journal of Chengdu University of Information Technology 31(6): 645-650.
[52] Zhao, T. B., Chen, L., Ma, Z. G. (2014): Simulation of historical and projected climate change in arid and semiarid areas by CMIP5 models. – Chin. Sci. Bull. 59(12): 412-429.
[53] Zhao, Y. Q., Xiao, D. P., Bai, H. Z. (2019): Projection and application for future climate in China by CMIP5 climate model. – Meteorological Science and Technology 47(4): 608-621.
[54] Zhou, B. T. (2021): Global warming: scientific progress from AR5 to AR6. – Trans. Atmos. Sci. 44(5): 667-671.
[55] Zhou, B. T., Qian, J. (2021): Changes of weather and climate extremes in the IPCC AR6. – Climate Change Research 17(6): 713-718.
[56] Zhou, T. J., Chen, Z. M., Zou, L. W., Chen, X. L., Yu, Y. Q., Wang, B., Bao, Q., Bao, Y., Cao, J., He, B., Hu, S., Li, L. J., Li, J., Lin, Y. L., Ma, L. B., Qiao, F. L., Rong, X. Y., Song, Z. Y., Tang, Y. L., Wu, B., Wu, T. W., Xin, X. G., Zhang, H., Zhang, M. H. (2020): Development of climate and earth system models in China: Past achievements and new CMIP6 results. – Acta Meteorologica Sinica 8(3): 332-350.
[57] Zhu, H. H., Jiang, Z. H., Li, J., Li, W., Sun, C. X., Li, L. (2020): Does CMIP6 inspire more confidence in simulating climate extremes over China? – Adv. Atmos. Sci. 37(10): 1119-1132.